Topology and distinct features of flashing flow in an injector nozzle

I. K. Karathanassis[1,*], P. Koukouvinis[2] and M. Gavaises[3]

School of Mathematics, Computer Science and Engineering, City University London, Northampton Square, EC1V 0HB London, UK

[1]Ioannis.Karathanassis@city.ac.uk, [2]Foivos.Koukouvinis.1@city.ac.uk, [3]m.gavaises@city.ac.uk

*Corresponding author

Abstract. The effect of thermodynamic non-equilibrium conditions (liquid superheat) on the two-phase flow field developing inside an axisymmetric, single-orifice nozzle is numerically investigated by means of different variations of a two-phase mixture model. A number of "hybrid" mass-transfer models that take into account both the effect of inertial forces (cavitation) and liquid superheat have been proposed and evaluated against widely-used, pure-cavitation models, in order to pinpoint the flow conditions necessary for flash boiling to occur and to elucidate the distinct features of the phase and velocity fields that characterize flashing flows. The effect of the number of nucleation sites, required as an input by the models, on the developing two-phase flow has also been looked into. The numerical results have shown that incorporation of an additional term corresponding to liquid superheat into the mass-transfer rate leads to increased evaporation rate, compared to pure-cavitation models with liquid vaporization taking place within the entire nozzle cross-section. The cavitation nucleation sites have been confirmed to act as the necessary flow perturbations required for flash boiling to occur. In addition, the developing velocity field has been found to be in close correlation to the mass-transfer rate imposed. It has been established that increased liquid evaporation leads to choked-flow conditions prevailing in a larger part of the nozzle and accompanied by a more significant expansion of the two-phase mixture downstream of the injector exit that results to increased jet cone angle. Finally, the results demonstrated that liquid

cooling due to the increased mass -transfer rate is not significant within the nozzle and thus considering a constant liquid temperature produces adequately accurate results with a decreased computational cost.

Keywords: two-phase flow, numerical models, thermodynamic non-equilibrium, cavitation, mass-transfer rate.

NOMENCLATURE

a	volume fraction	T	temperature, K
a	thermal diffusivity, m^2/s	t	time, s
c	speed of sound	u	axial velocity, m/s
C_p	specific heat, J/kgK		
h	heat transfer coefficient, W/m^2K	**Greek letters**	
h_{fg}	latent heat, J	ρ	density
Ja	Jakob number		
k	thermal conductivity, W/mK	**Subscripts**	
L	latent heat, J/kg	l	liquid
M	Mach number	mix	mixture
Nu	Nusselt number	nuc	nucleation
p	pressure, Pa	sup	superheat
R	bubble radius, m	sat	saturation
R_e	evaporation rate, kg/m^3s	v	vapour
R_c	condensation rate, kg/m^3s		

1. Introduction

Cavitation and flash boiling (flashing) are common phase-change processes realized in many engineering applications. Both processes are associated with vapour production due to liquid pressure drop below the saturation pressure at the given liquid temperature. In this case the required latent heat for the production of vapour is supplied as sensible heat coming from the cooling of the liquid. Referring to cavitation, vapour generation is accompanied by subsequent vapour condensation due to the increasing liquid pressure at later stages. However, in the case of flash boiling, the liquid pressure does not recover above the saturation pressure at the liquid temperature at any stage of the process. Furthermore, cavitation can be characterized as a pressure-driven process, whereas flash boiling is thermally driven, as the rate of bubble growth is designated by the heat transfer rate from the surrounding liquid into the bubble.

There are a number of studies available in the literature focusing on the growth rate of a bubble due to thermal effects considering conditions of thermodynamic equilibrium (Forster and Zuber, 1955; Zwick and Plesset, 1955; Scriven, 1959; Prosperetti and Plesset, 1978), i.e. that the vapour temperature within the bubble is equal to the respective temperature at the bubble interface. However, a necessary condition for the onset of flash boiling is the liquid transition to meta-stable (non-equilibrium) conditions. A general overview of the prevalent macroscopic features and the underlying thermodynamic processes associated with flashing flows can be found in the review article of Sher et al. (2008). In the case of a process that causes rapid liquid depressurization, the local liquid temperature can be higher than the saturation temperature at the specific pressure. This dynamical unstable condition, will cause the liquid to cool until it reaches its saturation

temperature, while the bubble grows due to the incoming heat from the surrounding liquid. There are few studies available that focus on the bubble-growth rate due to the effect of the thermal non-equilibrium (Theofanous et al., 1969; Jones and Zuber, 1978). Theofanous et al. (1969) and Jones and Zuber (1978) theoretically analyzed the mechanisms contributing to bubble growth in a varying pressure field and report correlations for the increased evaporation rate compared to thermal equilibrium conditions.

Negro and Bianchi (2011) distinguished the flash-boiling mechanism to internal and external depending on the location of initial bubble nucleation. In regards to internal flashing their simulations demonstrated that the flow reaches chocking conditions within the nozzle due to the increased mass transfer rate owing to the liquid superheat. A recent visualization study performed by Zhang et al. (2015) on a two-dimensional transparent nozzle confirmed that flashing conditions associated with liquid superheat are manifested through nucleation and bubble growth. It must be pointed that cavitation-induced bubbles were not present within the nozzle as the flow was kept laminar ($Re<1000$).

Occurrence of flash boiling inside injector nozzles is considered to have significant impact on their operation, as it has been demonstrated to lead to enhanced jet atomization, reduced penetration and increased spray-cone angle. Oza (1984) performed an experimental study focusing on flashing jets and reported as a main conclusion that depending on the ratio of the outlet-chamber pressure to the respective flow-inlet pressure, the jet could be either atomized within or at the nozzle outlet respectively. It was pointed out that the two atomization regimes could be discerned by the cone angle of the spray formed downstream of the nozzle, as in the cases where atomization occurs within the nozzle the jet exhibits an increased cone angle. In an additional experimental study of heated jets being expelled in a low pressure environment, Reitz (1990) observed that even

for liquid temperatures close to the saturation temperature, a liquid core exists until the exit of the injector nozzle, where the jet core rapidly breaks up due to the large difference between the saturation and atmospheric pressures. It was concluded that jet atomization does not take place within the nozzle for none of the cases investigated. A numerical study referring to the experimental case of Reitz (1990) has been performed by Gopalakhrishnan and Schmidt (2008), who used the Homogeneous Relaxation Model (HRM) model implemented in OpenFOAM for their simulations. The HRM model has also been employed by Saha et al. (2015) to predict the two-phase flow emerging in the nozzles of a gasoline multihole injector under different operating conditions.

The schlieren visualization of an externally-flashing, pure liquid jet performed by Vieira and Simões-Moreira (2007) demonstrated that increasing the degree of superheat reduces the jet-extinction length downstream of the nozzle outlet in an exponential manner due to more intense vaporization. More recently Serras-Perreira et al. (2010) experimentally examined the flow mechanisms that influence the degree of atomization of a jet exiting an injector nozzle. The investigation was conducted in a transparent-injector configuration for various hydrocarbon fuels. It was concluded that in the case of high-temperature fluids, the degree of liquid superheat designates the efficiency of jet atomization, while the cavitation bubbles act as nucleation sites for flashing to commence.

The studies of Senda and Hojyo (1994) and Price et al. (2015) concur that the occurrence of flashing flow is always accompanied by more efficient atomization of the spray exiting the nozzle. Aleiferis et al. (2010) reported that fuel sprays characterized by a high degree of superheat were visualized with cores of lighter colour indicating high concentration of vapour and fine droplets within the spray. The connection between the production of a spray comprising finer droplet

distribution and increased cone angle with the injection pressure and/or fuel temperature has also been reported by Chan et al. (2014). These findings are in agreement with the mechanism proposed by Lamanna et al. (2014) and supported by their experimental findings, according to which a rapid liquid depressurization leads to nucleation within the orifice and uniform bubble distribution in the liquid. Furthermore, the findings of Lamanna et al. (2014) demonstrated that the spray lateral spreading is controlled by the in-nozzle bubble nucleation.

The experimental data available in the literature are not in clear agreement in regard to the conditions that lead to flash boiling, as in some cases (Oza, 1984; Serras-Pereira, 2010; Zhang, 2015) it is argued that flashing occurs inside the injector nozzle, owing to the local state of the liquid due to the rapid depressurization and the density of the nucleation sites, while there are also experimental data suggesting that, for similar conditions, the liquid atomization commences at the injector outlet (Reitz, 1990; Vieira & Simões-Moreira, 2007). The present investigation aims to shed light on various aspects of the two-phase nozzle flow, such as the connection between the mass-transfer rate and the flow expansion downstream of the outlet that has led, until now, to ambiguity in the interpretation of experimental results. A number of mass-transfer models considering both inertial forces and thermal non-equilibrium effects have been formulated and implemented in the framework of a two-phase mixture model. The next paragraph discusses in detail the formulation of the numerical models proposed, while the subsequent sections present the model predictions in regard to the phase, velocity and temperature fields emerging in the injector configuration. The major findings of the study are summarized in the conclusions section.

2. Formulation of the numerical model

2.1 Geometry and thermophysical properties

As the main objective of the present study is to elucidate the flow mechanism that facilitates the emergence of flash boiling, an injector device of simple geometrical arrangement has been selected for the numerical simulations, in order to exclude any significant flow perturbations induced by the geometrical layout. The device in question (see inset of Fig. 1) is a simple axisymmetric injector nozzle with and abrupt (step-wise) reduction of the flow passage and geometrical dimensions identical to the device used in the experimental investigation of Reitz (1990). Since the distinct features of the two-phase flow field and the topology of the jet exiting the injector have been reported by Reitz, the configuration constitutes an ideal benchmark device for the characterization of the influence of thermodynamic non-equilibrium on the flow development.

Water has been used as the working medium with temperature in the range 360-430K, once again, as dictated by the experiments of Reitz (1990). Since there are various data bases giving water characteristics and, more importantly, since the evaporation pressure, which is a function of the inlet water temperature, is crucial for the flow process, in the following paragraphs the vapour pressure used in the simulations will be reported along with the inlet liquid temperature. It must be pointed out that the IAPWS tables (Wagner and Pruss, 2002) have been used in the present study for the calculation of the thermophysical properties of water, which. The tables cover the temperature range 273.16K - 647.096 K and therefore the liquid temperature range in the cases

investigated lies well within the range of available data. During preliminary simulations, it was verified that the numerical results are highly sensitive to the values assigned to the liquid saturation pressure (and vice versa to the saturation temperature). The designation of low-accuracy values, e.g. through the use of Antoine's law, leads to overestimation of the mass transfer rate within the nozzle and consequently, since the velocity field is closely connected to the phase field, to over-prediction of the flow velocity especially downstream of the nozzle outlet. For this reason, the pressure and temperature saturation values provided by the IAPWS tables were fitted using high-order polynomials and taken into account in the simulations.

In terms of an experimental investigation, it is of vital importance the exact operating conditions to be accurately reported. The water used in the experiments of Reitz (1990), which will be used as a reference for validating the numerical models, has not been categorised with regards to solid impurities and tensile stress as a function of temperature; therefore there is ambiguity in reference to the evaporation pressure as function of temperature, a parameter of basic importance for the predictions. The thermophysical properties of water have been evaluated at each one of the temperatures examined and treated as constant, since the temperature variation within the nozzle is expected to be rather insignificant.

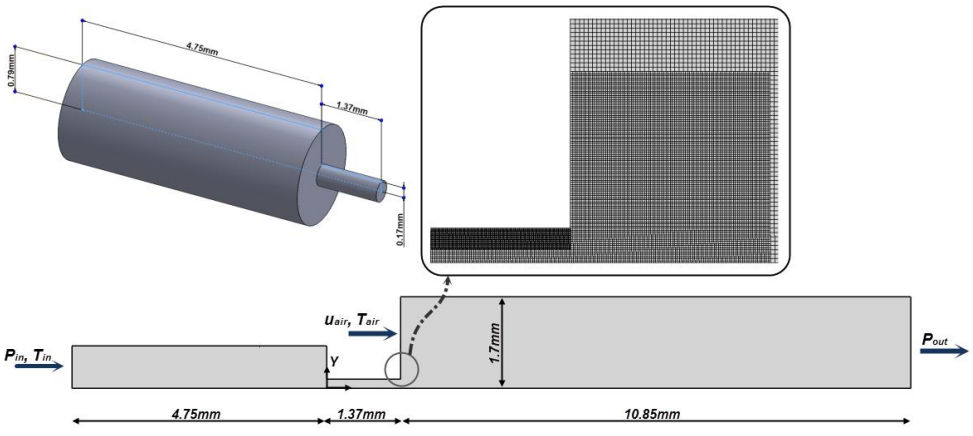

Fig. 1 Computational domain employed for the numerical model.

2.2 Computational domain and governing equations

An axisymmetric two-dimensional computational domain has been selected for the simulations (Fig. 1). A three-dimensional instability is unlikely to occur in the case of attached cavities that show no tendency of shedding (sheet cavitation), which have been verified to emerge in the present case. A three-dimensional cavitating flow topology has been reported to occur in the regime of cloud cavitation, however it is usually accompanied by a shedding mechanism manifested at the trailing edge of the attached vapour pocket. The fact that the mass flow rate is accurately predicted, as will be demonstrated in the following paragraph, constitutes additional proof that the use of a 2D axisymmetric domain does not obscure the topology of the actual flow field. It must be noted that the domain has been extended by several nozzle diameters downstream of the injector outlet, in order to make sure that the outlet boundary condition has not effect on the flow field emerging within the nozzle. In addition, the domain has been extended along the radial dimension (see also the inset of Fig. 1) to allow the un-perturbed formation of the jet cone downstream of the injector outlet.

Domain discretization was performed using a purely hexahedral (structured) grid, as depicted in Fig. 1. Telescopic local grid refinement methodology allowed the creation of a fine grid in the nozzle area (entrance and exit) allowing the capture of the distinct flow details. An additional zone of grid refinement was placed in the vicinity of the throttle wall in order to accurately capture the extent of the attached cavity. The total number of grid cells for the cases simulated was equal to 87781, while the y-plus values were maintained in the order of 1 along the throttle wall. A further refinement of the grid to 128847 cells was performed, in order to verify the independence of the solution from the grid employed. Considering a case of purely-cavitating flow at T=430K, the

maximum-velocity value at the injector outlet and the average vapour volume-fraction value at the throttle wall differed by 0.54% and 0.51%, respectively, compared to the respective values produced by the coarser grid. As shown in Fig. 2, the distribution of the vapour volume fraction at the throttle wall (Fig. 2a), as well as the radial velocity profile at the injector outlet produced using the fine grid (128847 cells) did not show any non-negligible variation in comparison to the respective produced using the initial grid (87781 cells). Hence, the grid comprising 87781 cells was considered adequate for the production of the presented results. For the flow conditions prevailing within the nozzle, the Taylor length scale was found to be equal to $5.2 \cdot 10^{-6}$ m, while the cell size at the region of mesh refinement, namely at the throttle, was equal to $4.25 \cdot 10^{-6}$ m, an indication that the specific grid density was suitable even for an LES study. However, a full three-dimensional grid of such density would have an overall cell number in the order of $20 \cdot 10^{6}$. For this reason, URANS models and a two-dimensional domain were employed in the present study and thus all turbulence length scales were modelled and not directly resolved. The overall number of cells used for the discretization of the nozzle internal region was equal to 24910, while 80 cells were placed across the throttle cross section.

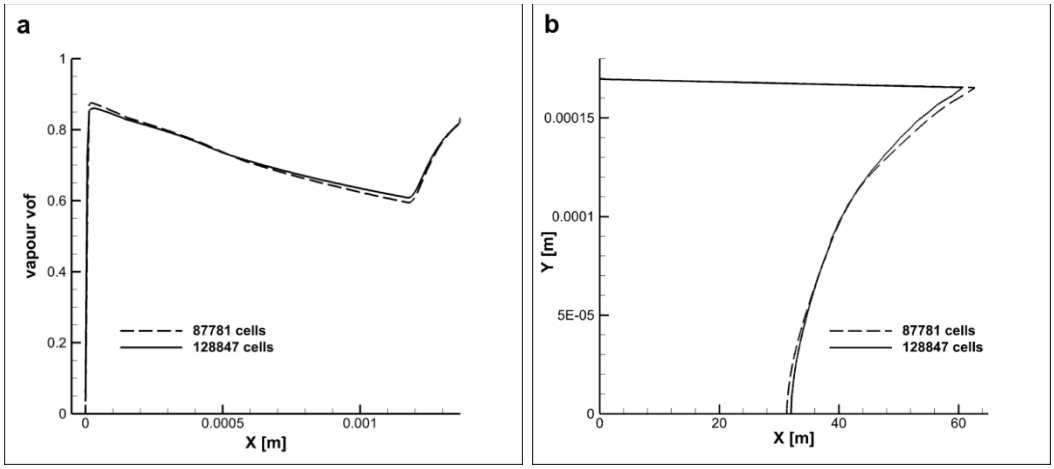

Fig. 2 Effect of the grid density on the produced results: (a) vapour volume fraction (vof) at the throttle wall ($Y=1.7 \cdot 10^{-4}$m) and (b) velocity profile at the injector outlet ($X=1.37 \cdot 10^{-3}$m).

To simulate the multiphase flow inside the injector an implicit, transient, pressure-based solver was used. Turbulence effects were accounted with the k-omega SST model, since the Reynolds number defined on the basis of the maximum flow velocity within the nozzle, for a case of "cold" flow (T=370K), was found to be approximately equal to 43000. The k-omega SST model is generally considered suitable for cases where flow separation and re-attachment are expected to occur. In addition, it has been demonstrated to be more accurate than the standard k-ε model in predicting the cavitating flow within complex geometries (Papadopoulos and Aleiferis, 2015).

It has been reported that RANS models are not capable of predicting a cavity-shedding pattern (Dular and Coutier-Delgosha, 2009) and furthermore that their validity could be situational in cases of incipient cavitation (Naseri et. al, 2015). However, RANS models have been found adequate to accurately predict cavitating flow in the cases of well-established, attached cavity pockets (Edelbauer et al., 2014) or even in injector flows (Andriotis et al., 2008). In the cases investigated in this study, the emerging cavity pocket is well-established and attached to the throttle wall and, furthermore, no shedding mechanism has been detected. Hence, the use of a URANS model is justified. In order to account for the enhancing effect of turbulence, which promotes instabilities in the shear layer, on the occurrence of cavitation, a correction equal to $\frac{1}{2}(0.39k\rho)$ has been added to the calculation of the vaporization pressure (see e.g. Singhal et al, 2002), with k being the turbulence kinetic energy.

Besides, phase-change effects were captured with the use of a two-phase mixture model. The two-fluid Eulerian model has also been for the simulation of two-phase flows (Battistoni et al., 2014; Habchi 2015), since it offers generality of the solution, as the pressure and velocity fields are resolved for each phase, however it is associated with additional computational cost and

increased risk of numerical instability compared to the mixture model, since a set of governing equations must be solved for each of the two phases. However, the use of the mixture model has been proven adequate for predicting cavitating/flashing flows (Battistoni et al., 2015; Schmidt et al., 2010), even high-velocity compressible flows within complex geometrical layouts (Koukouvinis et al., 2016). Hence, the use of a single-fluid model is justified in replicating a two-phase distribution by a density ratio, provided that the grid resolution is fine enough.

The coupled pressure/velocity solver implemented in FLUENT (v. 14.5) was used, in order to maximize computational stability, with second order schemes for turbulence advection and momentum. Although, the flow is expected to reach a steady-state solution, the transient solver was employed with a time step of $1 \cdot 10^{-6}$s, in order to improve the convergence of the solution. The time step selected in combination to the grid resolution produces a CFL number in the order of 4 in the nozzle region, a value that can be easily handled by the implicit solver employed for the simulations. It must be pointed out that the objective of the present investigation is not to resolve the highly-transient characteristics of the cavitating/flashing flow but rather to highlight the features of the averaged flow field, in order to illustrate the factors responsible for the different "steady"-flow behaviours observed downstream of the nozzle outlet in a number of experimental studies.

The two-phase mixture model, assumes mechanical equilibrium between the two phases, i.e. both liquid and vapour phase share the same pressure and velocity fields. In addition to the continuity and momentum equations, where terms corresponding to the contribution of mass transfer are added (ANSYS FLUENT, 2012), an advection equation corresponding to the vapour fraction is solved, in the following form:

$$\frac{\partial(a\rho_v)}{\partial t} + \nabla(a\rho_v \mathrm{u}) = R_e - R_c \tag{1}$$

where a is the vapour fraction, ρ_v is the vapour density, **u** is the velocity field and R_e, R_c are the mass transfer rates for condensation (c) and evaporation (e). The latter terms are associated with semi-empirical bubble dynamic models, based on a simplified form of the Rayleigh-Plesset equation (Brennen, 2005). Both the liquid and vapour phases are treated as incompressible, however, it must be highlighted that even if the individual phases are incompressible, the mixture is not, since mass transfer is involved; actually, the mass transfer is the dominant term affecting the value of the speed of sound c for the mixture and thus it compressibility, as indicated by the following relation (Franc and Michel, 2005):

$$\frac{1}{\rho_{mix} c_{mix}^2} \approx \frac{a}{\rho_v c_v^2} + \frac{1-a}{\rho_l c_l^2} + \frac{(1-a)\rho_l Cp_l T}{(\rho_v L)^2} \tag{2}$$

where L is the latent heat of vaporization. Considering only the third term on the right-hand side of Eq. (2), e.g. for a low- (T=370K) and a high-temperature (T=430) simulation case included in this study, the overall discrepancy in the mixture sound velocity (for the different values of the vapour volume fraction) was calculated to be in the order of 0.5% and 1.5%, respectively, compared to the full expression comprising all three right-hand-side terms.

The energy equation has also been solved for some of the cases presented in the next paragraph. A source term of the form $S=R_e \cdot h_{fg}$ has been subtracted from to the energy equation corresponding to the liquid phase and respectively added to the respective equation of the vapour phase to account for the latent heat h_{fg} required for the evaporation process.

Suitable boundary conditions were supplied for the governing equations, in order to numerically replicate the flow conditions prevailing during the experimental investigation of Reitz

(1990). Constant pressure values, equal to $7.98 \cdot 10^5$ Pa and $1.1 \cdot 10^5$ Pa, respectively, where imposed at the domain main-flow inlet and outlet, as depicted in Fig. 2:

$$\begin{aligned} &\textit{Inlet:} && p=p_{in} \\ &\textit{Outlet:} && p=p_{out} \end{aligned} \tag{3}$$

In order to closely follow the experimental conditions of Reitz (1990), an additional inlet, also evident in Fig. 2, has been placed on the edge above the nozzle outlet from which pure vapour enters the domain. Reitz (1990), in his experiments used a stream of air to avoid early disintegration of the jet exiting the injector and to facilitate the jet visualization. The mass flow rate of the vapour stream set for the simulations has been calibrated, so as to match the respective air mass flow rate reported in the experiments:

$$\textit{Vapour inlet:} \qquad \dot{m} = \dot{m}_{air} \tag{4}$$

All the other outer edges of the domain, apart from the axis of rotation (Y=0), were treated as walls and the no-slip condition was imposed:

$$\textit{Outer edges:} \qquad u=0 \tag{5}$$

At initial conditions, the vapour fraction was assumed to be equal to zero in the entire domain, while the pressure was set equal to the inlet pressure. Calculations were carried out until it was confirmed that a steady solution had been reached. A flow time of 2.5 ms was found to be sufficient to declare steady-flow conditions corresponding to a simulation time of approximately two hours in a 12-core machine.

2.3 Mass-transfer models

The cavitation models tested in the framework of the present analysis are those formulated by Schnerr and Sauer (Yuan, Sauer, and Schnerr 2001), Zwart, Gerber and Belamri (ZGB) (2013) and Singhal et al. (2002). The models provide the rate of mass transfer, which is based on the rate of change of the vapour bubble radius *dR/dt* derived by the solution of the simplified Rayleigh-Plesset equation, where the surface tension and viscous forces, as well as the higher-order terms are neglected:

$$\frac{dR}{dt} = \sqrt{\frac{2}{3\rho_l}[p_{sat}(T_l) - p]} \tag{6}$$

This approximate expression for the bubble growth (or collapse) velocity is used in conjunction with semi-empirical tuning parameters accounting for factors such as the number of nucleation sites, the effect of gas content and the turbulence intensity in order to calculate the mass transfer rate. Especially in order to account for the nucleation-site density, a fixed number of sites per unit volume, considered to encompass the effect of both water impurities and wall roughness on bubble nucleation, was assigned for each simulated case. It is important to mention that the formulation of the Schnerr-Sauer and ZGB models bear significant resemblance and mainly differ in the assumption employed for the determination of the nucleation-site density during the early phases of bubble growth. Unlike the aforementioned models, the Singhal et al. model also takes into account the effects on non-condensable gas and turbulence intensity on the mass-transfer rate. The above models assume that the generated vapour is always at saturated conditions.

2.4 Validation of the numerical model

A comparison of the numerical predictions of the cavitation models employed, for different values of the model parameters, with the available experimental data of Reitz (1990) for the variation of the inlet mass flow rate in proportion to fluid temperature is presented in Fig. 3a. It can be discerned that the best approximation is obtained by the Zwart-Gerber-Belamri model, considering a somewhat decreased mass transfer rate imposed to the model by increasing the initial bubble diameter from 10^{-6} to 10^{-4} m, a tuning parameter in the formulation of the model, which in reality corresponds to a reduction of the bubble density number (or available nucleation sites) from 10^{13} to 10^{7} sites per liquid volume unity. The ZGB model ($R_b=10^{-4}$ m) closely follows the trend of the experimental data, with the average discrepancy being less than 5%, which is estimated to be close to the experimental uncertainty (although it is not reported by Reitz). The flow rate is decreased by approximately 15% in the temperature range considered (370-430K). As the extent of the nozzle cross-sectional area occupied by vapour increases, the available active area for the liquid to flow decreases and consequently the inlet mass flow rate decreases as well. Besides, the ZGB and Schnerr-Sauer models that neglect the effect of gas content on mass-transfer rate produced results in closer agreement to the experimental data. Therefore, it is justified to deduce that the effect of gas content does not have a significant effect on the two-phase flow within the nozzle. It is interesting to notice that both the Schnerr-Sauer and ZGB models, if a bubble radius of 10^{-6} m is considered, predict a much steeper decrease of the flow rate for the examined temperature range, since the mass flow rate at 430 K drops to approximately half of its respective

value at T=360 K and thus the considerable influence of the number of nucleation sites on the predicted mass transfer rate becomes evident.

It is reported by Reitz that a steep decrease of the inlet mass flow rate was detected for a liquid temperature equal to the saturation temperature, reported to be 432K. This abrupt decrease is predicted by the ZGB model, however at a temperature of 443K, which is the value of the saturation temperature corresponding to the inlet pressure according to the IAPWS tables.

Furthermore, a comparison in reference to the change of the inlet mass flow rate with temperature conducted between the predictions of the present study and the ones available by Gopalakrishnan and Schmidt (2008) showed a very good agreement (Fig. 4b). The Homogenous Relaxation Model employed by Gopalakrishnan and Schmidt (2008) is based on the concept of a characteristic time period required for the flow to transit to thermodynamic equilibrium and has been validated against available experimental data in a number of studies focusing cavitating/flashing flows (Battistoni et al. 2015; Lee et al., 2009; Schmidt et al., 2010). It should be noted that in the present case the fluid thermophysical properties were taken from IAPWS tables, while the REFPROP software was used in (Gopalakrishnan and Schmidt, 2008). It is therefore reasonable to conclude that valid properties have been applied for both the liquid and vapour phases. Thus, the discrepancy in the fluid temperature value, where the steep decrease of the flow rate takes place, evident between the experimental data and both numerical studies could be therefore attributed to a mismatch between the actual thermophysical properties of the fluid used in the experiments of Reitz (1990) and the reported values.

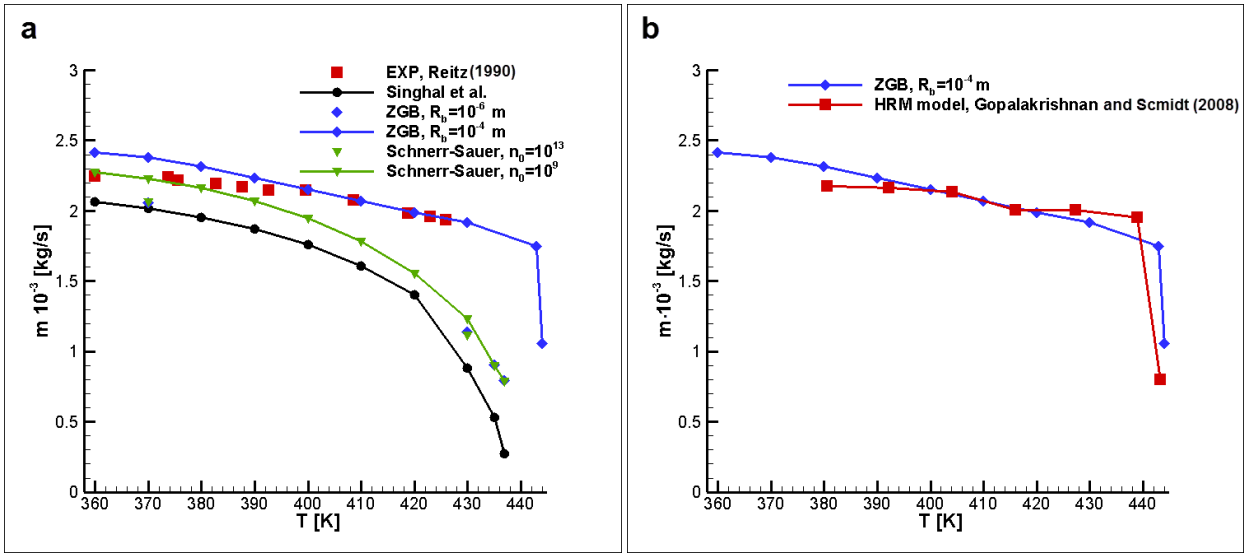

Fig. 3 Comparison of the inlet mass flow rate predicted by the various cavitation models: (a) with the experimental data published by Reitz (1990) and (b) with the numerical predictions of Gopalakrishnan and Schmidt (2008).

An additional validation study was performed in order to demonstrate that the ZGB model, which produced more accurate predictions compared to the two other models employed, in reference to the Reitz nozzle layout, is, in general capable of predicting cavitating flows. The predictions of the model were compared against the experimental data provided by Sou et al. (2007) who visualized the development of cavitating flow in a two-dimensional throttle, as well as the topology of the spray downstream the throttle outlet. Water at a temperature T=333K was considered as the working medium for the test case used for the validation of the model predictions. As depicted in Fig. 4a, the predictions of the ZGB model regarding the length of the emerging cavity (non-dimensionalized with the throttle length) are in close agreement with the experimental data and the steep increase of the cavity length, as the Reynolds number increases, is well captured.

Fig. 4b depicts the comparison of the model predictions with the experimental data for the cone angle of the spray exiting the throttle. Although the increasing trend of the angle with the cavity

length is captured by the model, a discrepancy can be detected between the numerical predictions and the experimental data. Nevertheless, the experimental measurement is expected to be associated with significant error, as the angle was determined by measuring the width of the visualized spray at a specified location downstream the throttle outlet. Since the spray did not have a clear interface and the values of the angles are very small, the values reported by Sou et al. (2007) should be treated as indicative. The extensive validation of the ZGB model justifies that the model is capable of accurately predicting two-phase flows in throttle geometries.

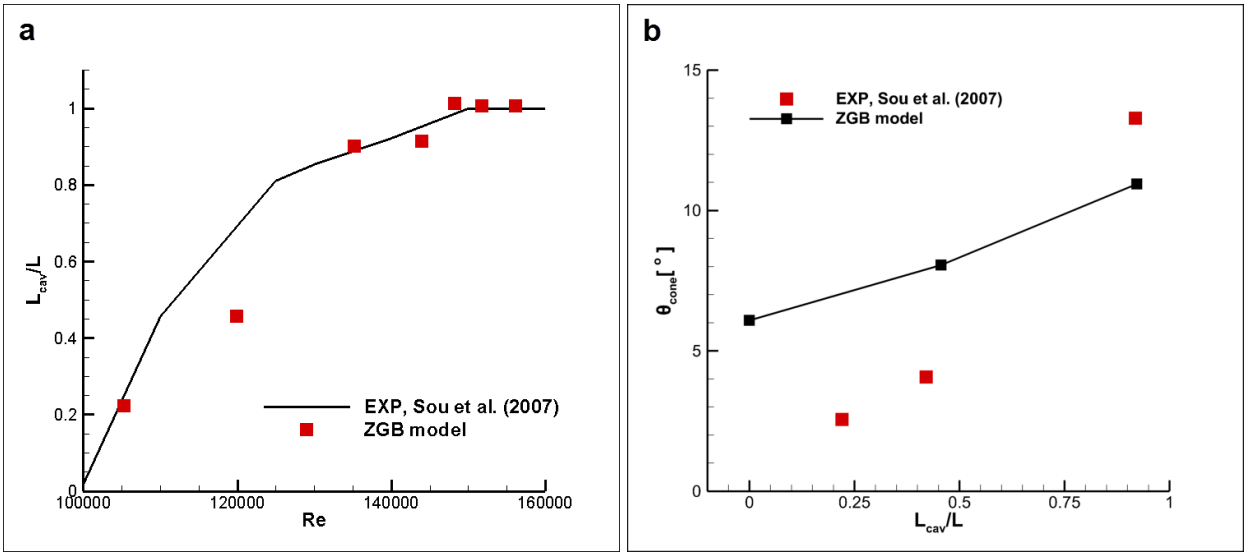

Fig. 4 Comparison of the predictions of the ZGB model with the experimental data of Sou et al. (2007): (a) cavity length and (b) jet cone angle.

2.5 Thermodynamic non-equilibrium- Effect of liquid superheat

The conventional formulation of the Rayleigh-Plesset equation suggests that the driving force for bubble growth is the difference between the saturation (vapour) and liquid pressures. However, it is postulated that the vapour temperature inside a growing bubble is equal to the temperature at the bubble interface, i.e. thermodynamic-equilibrium conditions exist. However, the rate at which

the phenomenon takes place can have a fundamental impact on the evaporation mechanism, since, as reported by Sher et al. (2008), a faster process leads to a more violent liquid vaporization.

The process undergone by a rapidly depressurizing liquid can be further elucidated, if Fig. 5 is considered, i.e. the pressure-volume diagram of a pure fluid. A sub-cooled liquid at an initial pressure p and temperature T_2 transits isothermally to a lower pressure, where, although its pressure is equal to the saturation pressure p_{sat}, its temperature is higher than the (boiling) temperature T_1 corresponding to the saturation pressure. Therefore, its thermodynamic state lies between the saturation and spinodal lines (where $\left({}^{\partial p}/_{\partial v}\right)_T = 0$), in the region of meta-stable liquid. The degree of superheat is defined as $\Delta T_{sup}=T_2-T_1$. In terms of bubble growth, the effect of thermodynamic non-equilibrium is manifested as a temperature discontinuity at the bubble interface, assuming that the vapor inside the bubble is at saturated conditions (p_{sat}, $T_{sat=}T_1$ referring to Fig. 5), whereas the temperature at the interface is equal to that of the superheated liquid ($T=T_2$). Hence, it can be concluded that the necessary mechanism for the liquid to transit back to a stable thermodynamic condition is, in essence, flash boiling, which is manifested through the formation of additional nucleation sites and bubble growth (Sher et al. 2008; Lee et al. 2009).

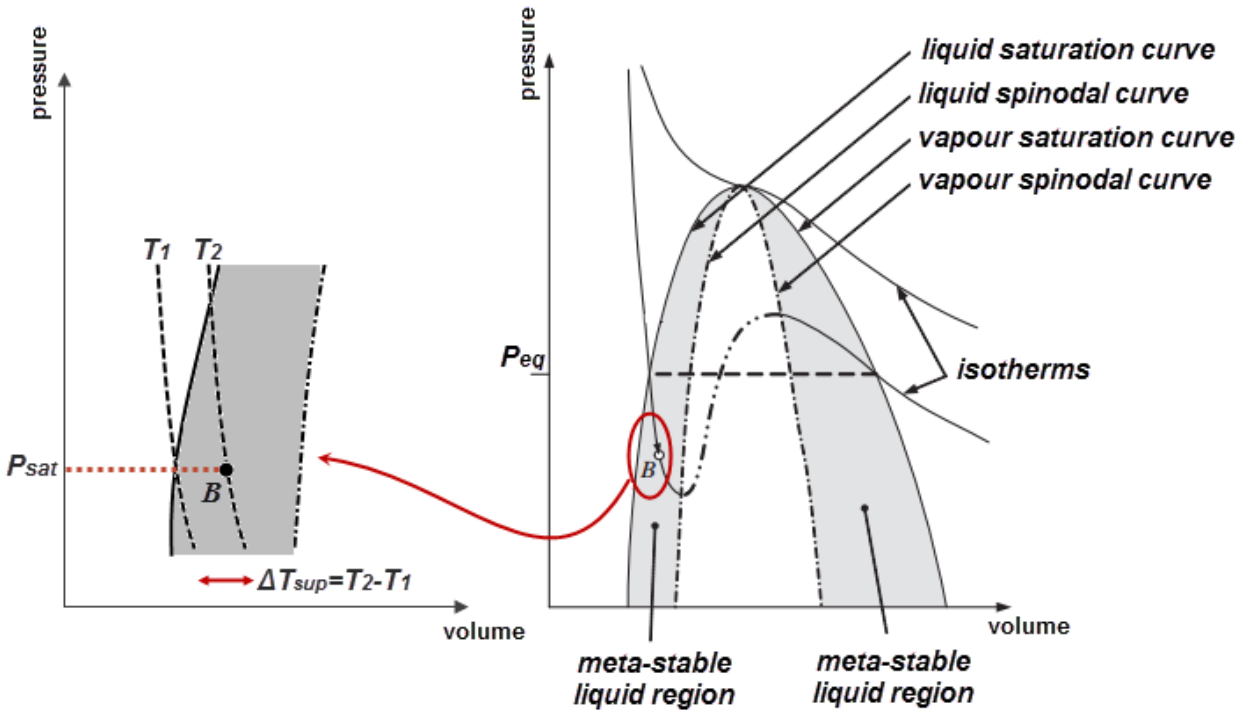

Fig. 5 Schematic of the pressure-volume diagram for a pure fluid (adapted from Sher et al. (2008)).

It is essential to clarify that although the bubble growth in the present flash-boiling cases is essentially thermally driven, it should not be confused with the limiting growth rate due to the cooling of the liquid boundary layer around the bubble under thermodynamic equilibrium conditions, as described by Brennen (1995). From a physical point of view, in the cases investigated, the growing bubble is not stationary but instead it is transferred by the main flow into regions of surrounding liquid, where no cooling due to vaporization has come into effect. Besides, it must be clarified that, since the mixture model is employed, the temperature field is considered common for the two phases. An assumption is made that the depressurization process is "rapid" enough to disrupt the thermal equilibrium in a way where the temperature at the bubble interface

is equal to that of the surrounding (superheated) liquid, while the temperature of the vapour inside the bubble is equal to the saturation value corresponding to the prevalent pressure.

A number of mathematical formulations realizing the additional non-equilibrium effect on the bubble-growth rate are proposed in the following section, based on the superheat definition explained above. The proposed relations contribute to the mass-transfer rate in an increasing manner and have been implemented within the code as User Defined Functions (UDFs). It must be noted that the ZGB model, which has been found to accurately capture the development of cavitation within the investigated geometry, has been considered as the basis for the formulation of the hybrid models that also take into account the effect of liquid superheat. According to the typical formulation of the model, the evaporation mass-transfer rate is calculated as:

$$R_e = F_{vap}\frac{3a_{nuc}(1-a)\rho_v}{R_b}\frac{dR}{dt} \quad (7)$$

where F_{vap} (=50) is a model emprical constant, a_{nuc} (=0.0005) is the nucleation site volume fraction and R_b is the bubble diameter . The correlations proposed by the authors and presented in the next paragraph modify the bubble-growth term *dR/dt*, in order the effect of the temperature difference at the bubble wall (thermal effect) to be taken into account.

2.5.1 Model I- Theoretical correlation for thermal bubble growth

The bubble-growth rate due to the thermal effects is considered constant according to the proposed model and added to the pressure-driven term (Eq. 6). Therefore this approximation corresponds to the upper limit of growth rate, as the local liquid cooling due to mass transfer rate is neglected. The added thermal term is derived under the concept of a growth constant *C*, as proposed by Forster and Zuber (1955) and, in essence, designates that larger bubbles grow slower:

$$\frac{dR}{dt}_{th} = \frac{C^2}{2R_b} \tag{8}$$

where R_b is the bubble diameter and the C constant is calculated by the following relation (Robinson, 2002; Scriven 1959):

$$C \approx 2\sqrt{3}\left(\frac{1}{1+\gamma}\right)(Ja)\left(\frac{\alpha}{\pi}\right)^{1/2}$$

$$\gamma = \frac{Cp_l - Cp_v}{h_{fg}}(T_l - T_{sat}) \tag{9}$$

$$Ja = \frac{\rho_l Cp_l (T_l - T_{sat})}{\rho_v h_{fg}}$$

where ρ_l, Cp_l, are the liquid density, and specific heat, while ρ_v, Cp_v and h_{fg} are the vapour density, specific and latent heat. T_l is the (superheated) liquid temperature and T_{sat} is the saturation temperature at the local pressure.

2.5.2 Model II- Heat-transfer designated growth-rate

The proposed model assumes that the bubble growth rate due to the additional effect of superheat is designated by the heat-transfer rate at the bubble interface. The energy balance at the interface can be formulated as follows:

$$\frac{dR}{dt}_{th} \rho_v h_{fg} = h(T_l - T_{sat}) \tag{10}$$

where *h* is the heat transfer coefficient defined on the basis of a Nusselt number value ($h=Nuk/2R_b$), which, in turn, is designated by the local Jakob-number value through a correlation proposed by Chang and Lee (2002):

$$Nu = 2 + \frac{12Ja}{\pi} + \left(\frac{6Ja}{\pi}\right)^{1/3} \tag{11}$$

2.5.3 Model III- Modified Rayleigh-Plesset equation

A modified formulation of the typical Rayleigh-Plesset equation is considered, where the bubble growth rate is determined as the weighted average between two limiting growth rates corresponding to inertial forces and non-equilibrium (thermal) effects respectively:

$$\frac{dR}{dt} = S_{Ja}\sqrt{\frac{2}{3\rho_l}[p_{sat}(T_l) - p]} + \left(1 - S_{Ja}\right)\sqrt{\frac{2}{3\rho_l}[p_{sat}(T_l) - p_{sat}(T_{sat})]} \tag{12}$$

The weighting factor S(Ja) is defined as:

$$S(Ja)=Min(1,Ja/12) \tag{13}$$

and actually acts as a limiter of the mass-transfer rate in the regions of minimum pressure where cavitation emerges. The formulation of the Rayleigh Plesset shown in Eq. (12) is proposed by the authors and it bears some similarity to the formulation of the Rayleigh-Plesset equation reported by Brennen (1995), where thermal effects are also taken into account. However, unlike the flow

conditions considered by Brennen, in the present case the bubble is considered to have been transported by the main flow to a liquid region with a certain degree of superheat and thus the bubble growth is enhanced due to thermal effects. For a conventional limit of *Ja=12*, thermodynamic equilibrium conditions are considered and Eq. (12) switches to its typical form for purely cavitating flows, while the influence of thermal non-equilibrium conditions comes into effect as the values decrease.

The conventional limit Ja=12 has been derived considering an estimation of the mean time period for which the bubble growth during a process is controlled by inertial forces, which according to Robinson (2002) is equal to *Ja/100* ms. For the geometrical layout and flow conditions regarding a high-temperature case (T>430, axial velocity in the order of 20 m/s in the throttle) of the present investigation, the inertial bubble-growth time becomes equal to the fluid residence time in the throttle for a mean value of Ja≈12. The concept of two vaporization mechanisms has also been considered for externally flashing jets, see e.g. (Senda et al. 1994; Price et al. 2015), while the concept of two limiting rates in regard to mass-transfer has also been demonstrated in the recent publication of Saha et al. (2015). It is essential to point out that unlike the two previous models, where the corresponding growth rates due to pressure and temperature difference are added, in this proposed model a prevailing mechanism is considered, which primarily designates the mass-transfer rate, depending the value of the Jakob number.

3. Results and discussion

The numerical predictions of the different model formulations are presented in this paragraph. The results shown in the following section were produced employing the pure-cavitation models and should be treated as a reference for the subsequent sections, which illustrate results obtained

with the use of the "hybrid" models. In this way, the added effect of liquid superheat on the developing flow field can be clearly elucidated.

3.1 Predictions employing the pure-cavitation models

The predictions of the cavitation models with regard to the phase field that emerges in the injector configuration are presented in a comparative manner in Fig. 6 for the two extreme values of the temperature range considered in the present investigation. As it is evident from the contour plots of the volume fraction for the lower temperature (T=370K), shown in Fig. 6a, cavitation occurs only in a localized region adjacent to the throttle wall and a liquid core exits the nozzle. It must be noted that the Singhal et al. model exhibits significant deviations from the other two models, as cavitation appears to be much more diffusive occupying almost the entire cross section of the nozzle. In reference to the ZGB and Schnerr-Sauer models, the bubble density number n_0 and the bubble radius R_b act as tuning parameters for the models and are responsible for adjusting the mass transfer rate, i.e. vapour production. The contour plots reveal that a lower bubbler density number or a smaller bubble radius (depending on the employed model) lead to decreased mass transfer and thus vapour of lower volume fraction in the region, where cavitation occurs.

Referring to the high-temperature case (T=430K), Fig. 6b, the predictions of the ZGB and Schnerr-Sauer models for $R_b=10^{-6}$ m and $n_0=10^{13}$, respectively, comply with one another and make evident that "flashing" of the entire liquid volume, occurs at the nozzle outlet. The abrupt increase in the rate of liquid phase-change process is owed to the significant difference between the inlet and back pressures and is in agreement with the overall observations of Oza (1984) and Reitz (1990) that superheated jets definitely break up when they enter a chamber of atmospheric pressure. Considering a reduced mass-transfer rate ($R_b=10^{-4}$ m or $n_0=10^{9}$) the fluid exits the nozzle

as a bubbly mixture, as the vapour volume fraction is close to 0.5, whereas for $R_b=10^{-6}$ m or $n_0=10^{13}$ the vapour volume fraction reaches values slightly below 1.0 shortly downstream of the nozzle outlet. The results of the two models clearly indicate that the smaller the number of inception sites (value of n_0) or the larger the initial bubble diameter (which for the same initial vapour volume fraction corresponds to fewer inception points), the lesser is the vapour production rate, revealing that accurate determination of the number of inception sites is vital for the accurate prediction of the phase field. Once again, the predictions obtained by the Singhal et al. model show that cavitation occurs almost in the entire nozzle region. Furthermore, the predictions of the Singhal et al. model reveal that downstream of the nozzle outlet the highest vapour fraction values (in the order of 0.7 for T=430K) are encountered exactly the channel core and that the vapour area is surrounded by regions of lower vapour fraction values (in the order of 0.20). This behaviour is in disagreement with the observations of Reitz who states that for cases with liquid temperature higher than 400K, where spray formation is observed, a liquid core exists at the channel central part surrounded by "a fine spray". Hence, it is concluded that the specific model fails to predict the evolution of two-phase flow in the specific nozzle configurations.

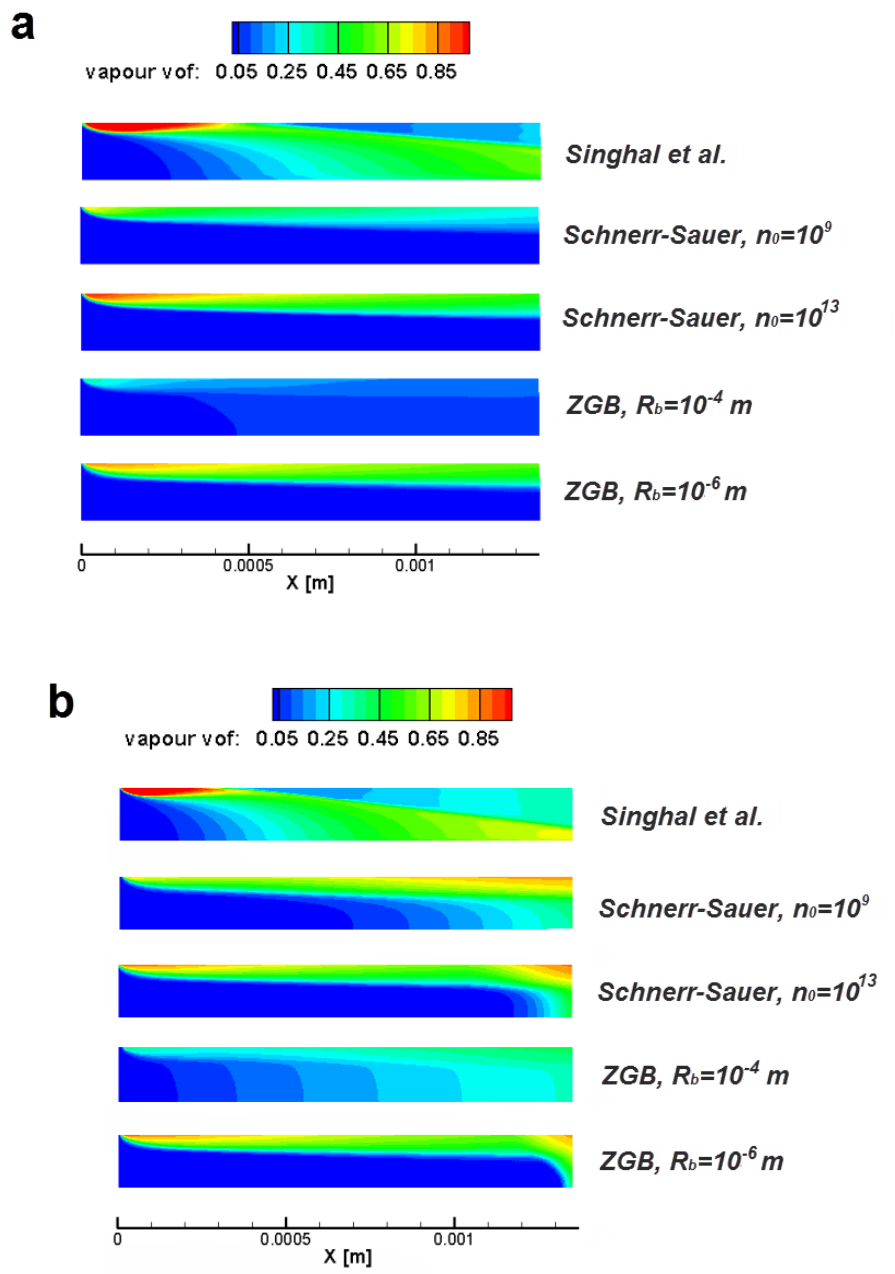

Fig. 6 Contour plots of the phase field (vof stands for volume fraction): (a) T=370K (p_{sat} =90540Pa) and (b) T=430K (p_{sat}=570260Pa).

Fig. 7 presents the axial velocity distribution at the injector exit for two inlet liquid temperatures, equal to 370K and 430K, respectively. At low inlet temperature (Fig. 7a), the liquid

core has an exit velocity around 38m/s, whilst at the outer part of the exit nozzle the vapour velocity is lower. Thus, the liquid core drives the outer vapor flow. At the elevated temperature (Fig. 7b), the "liquid core" occupies a small central area of the exit and has a velocity of 32m/s, whilst the external part of the injector outlet is occupied by vapor with much higher velocity; i.e. in this case the vapor flow drives the liquid core. It must be reminded that the velocity field is connected to the mass transfer rate through a source term added to the momentum equation. In reference to the Singhal et al. model, a more extended nozzle region occupied by vapour was predicted in comparison to the other models employed, as revealed by Fig. 6, leading to reduced flow velocity in the throttle region, as illustrated in Fig. 7b. Besides, in regard to the high-inlet liquid temperature case, if viscous heating is considered (kinetic heating) then a local increase of temperature at the stagnation point and at the inlet to the injector of around 1K is calculated, thus having a negligible effect on the flow development.

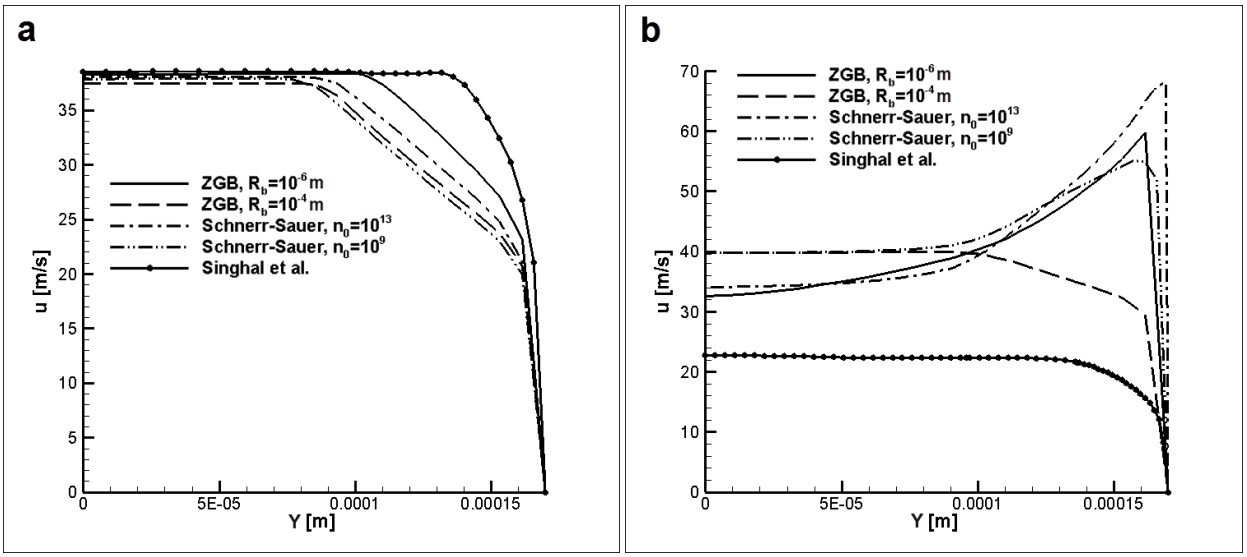

Fig. 7 Axial velocity profiles at the nozzle outlet: (a) T=370K (p_{sat} =90540Pa) and (b) T=430K (p_{sat}=570260Pa).

Fig. 8 shows the Mach number $M=u/c_{mix}$ (c_{mix} calculated using Eq. 2) distribution in the injector for the two cases, those of low and elevated liquid temperatures, for the ZGB model, while the respective predictions of the Schnerr-Sauer model are almost identical. Whilst for the low liquid temperature (Fig. 8a) the Mach number is rather low, ranging from almost 0.025 (liquid core) to 0.9 (region of mass transfer), as the inlet temperature increases (Fig. 8b) the local mach number approaches unity at the injector outlet, indicating flow chocking (Brennen, 2005). Due to the extensive evaporation taking place in the high-temperature case (Fig. 8b), the speed of sound in the mixture obtains values much lower than the respective for pure liquid or vapour, in the order of 35 m/s and hence the flow velocity becomes sonic in the vicinity of the outlet. The flow at the exit of the injector is expected to have a higher pressure than the outlet pressure and thus expansion waves might appear at the injector outlet.

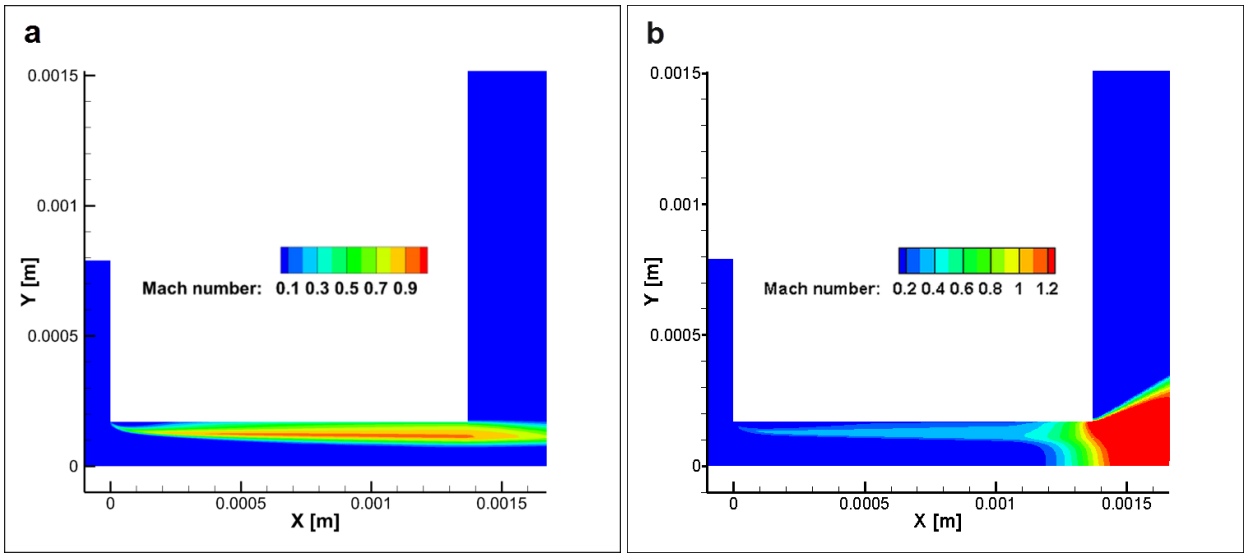

Fig. 8 Mach number distribution (ZGB model, $R_b=1.0\cdot10^{-6}$ m): (a) T=370K (p_{sat} =90540Pa) and (b) T=430K (p_{sat}=570260Pa).

As illustrated by the increasing Mach-number values discerned in Fig. 8b, the flow is accelerating in the vicinity of the nozzle outlet, since the increase, which is an indication of under-expanded flow within the throttle. This indication is verified by Fig. 9 depicting the pressure distribution both in the throttle region and downstream the injector outlet. Referring to the low temperature case T=370K (Fig. 9a), the pressure reduces to its atmospheric value in the vicinity of the geometrical constriction. However, in the high temperature (T=430K) case, the flow remains pressurized throughout the largest part of the throttle length, while a rapid depressurization occurs at the outlet region. The flow expansion downstream the injector outlet is associated with the formation of a shockwave and subsequently the pressure adjusts to the atmospheric value (see inset of Fig. 9b). The distinct flow features illustrated by Figs. 9-10, i.e. significant pressure drop at the outlet and flow acceleration, formation of a shockwave, clearly demonstrate that the flow is under-expanded within the throttle and its expansion downstream of the outlet will lead to an increased jet cone angle (Oza, 1984; Prudhomme and Haj-Hariri, 1994).

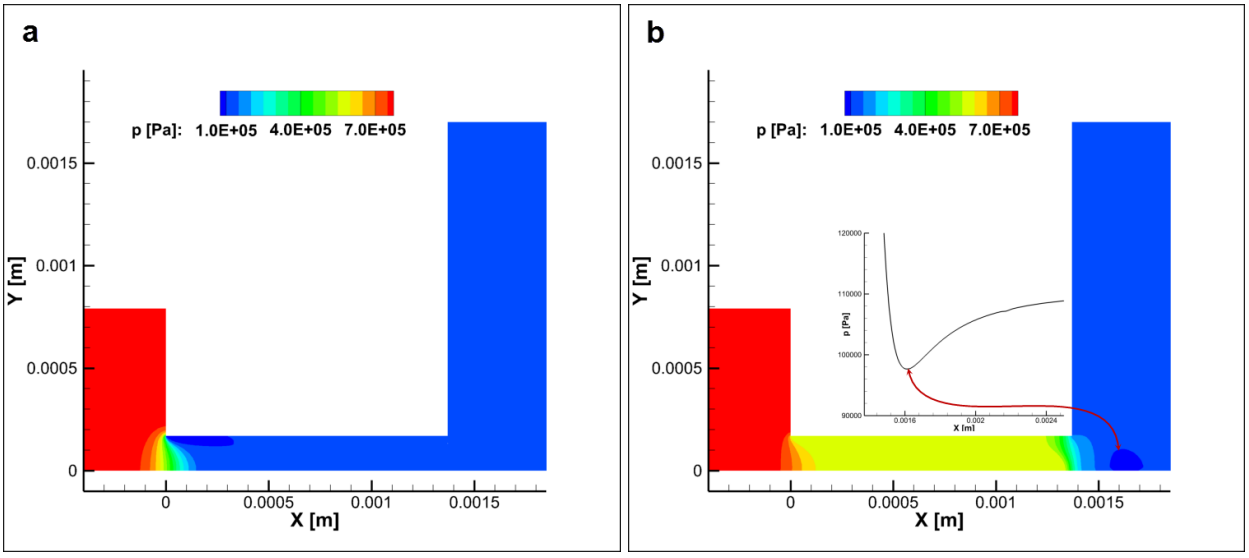

Fig. 9 Pressure distribution (ZGB model, R_b=1.0·10^{-6} m): (a) T=370K (p_{sat} =90540Pa) and (b) T=430K (p_{sat}=570260Pa).

3.2 Effect of the growth rate corresponding to non-equilibrium conditions

In all the cases presented until now, the effect of liquid superheat within the nozzle was neglected and the mass transfer rate was designated by the difference between the liquid local pressure and the vaporization pressure. Nevertheless, it has been reported by Oza (1984) that for back to inlet pressure ratios in the order of 0.1, spray atomization commences inside the nozzle. In order to predict this behavior, the additional term corresponding to thermodynamic non-equilibrium effects, which contributes to the bubble-growth rate has been implemented into the ZGB model.

The contour plots of Fig. 10 depict the predictions of the hybrid models regarding the phase field that develops within the injector nozzle, as well as slightly downstream of its exit. An observation that can be made regardless of the model employed is that more extensive mass transfer takes place within the nozzle in comparison to the pure-cavitation cases. The contour plots clearly illustrate that the liquid vaporization commences from the throttle vertex, which also acts as the inception point of the attached cavity, and gradually expands from the nozzle wall to the orifice main axis. This trend in the predicted vapour-fraction distribution is in compliance with the observations of Serras-Pereira et al. (2010), which report that the presence of cavitation-induced bubbles enables the onset of flash boiling. In other words, the vapour bubbles in the region close to the nozzle outlet, where the effect of liquid superheat is more significant, act as the flow perturbations necessary for intense nucleation, i.e. flash boiling, to commence. Thus, nucleation within the nozzle, where both pure-cavitation and flash-boiling conditions are in effect, could be characterized as a type of heterogeneous nucleation (Sher et al., 2008).

For T=430 K the mass transfer in the core region is relatively low due to the respective low degree of superheat calculated to be in the range 1.5–3.0 K in the largest part of the nozzle, giving respective Jakob numbers in the range 1.0-2.0. The resulting vapour volume fraction is in the range 0.1-0.3 depending on the formulation of the model. It can be discerned that Model II (Fig.10b) predicts a more extensive mass-transfer region in the channel core compared to the other two models. In addition, a close comparison between Figs. 6b and 10 reveals that the localized region of extensive liquid-core vaporization is shifted to locations upstream of the nozzle outlet, when non-equilibrium effects are taken into account. Similar to the cavitation cases, the high difference between the injection and back pressures leads to total jet disintegration shortly downstream of the injector outlet.

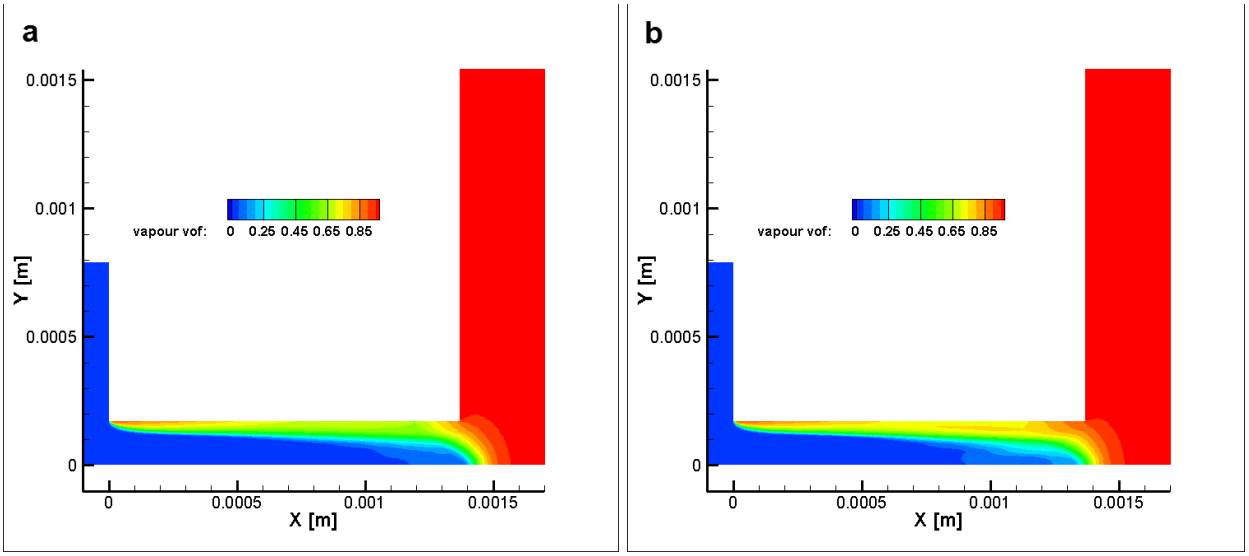

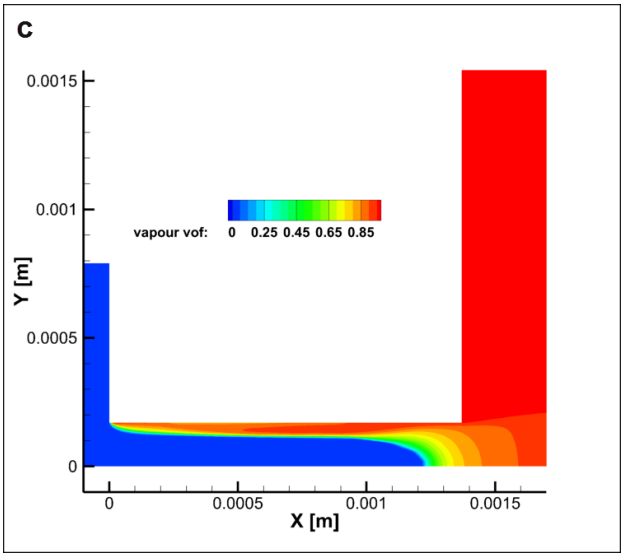

Fig. 10 Contour plots of the phase field at T=430K (ZGB-R_b=10^{-6}m): (a) Model I, (b) Model II, (c) Model III.

The distribution of the vapour volume fraction along the injector radial dimension at a specific location close to the injector outlet (X=0.0012m) is shown in Fig. 11 for three liquid temperatures. As clearly revealed, the mass-transfer rate in the channel-core region is controlled by the degree of superheat. As the liquid inlet temperature increases, a larger area of the channel core fills with vapour (as shown on the inset of Fig. 11b), while higher values of the vapour volume fraction are predicted along the entire nozzle radius at X=0.0012 m. The volume-fraction values predicted by Model III (Fig. 11c) are, in general, lower by the respective referring to Models I (Fig. 11a) and II (Fig. 11b). Yet this difference is justified, since according to the formulation of Model III, discussed in paragraph 2.5.3, the growth-rates due to the pressure and temperature difference act in a contradicting manner and not in combination, as in models I and II. Nevertheless, the pure liquid core predicted by the cavitation models at the injector outlet is clearly absent in the cases of flashing flow.

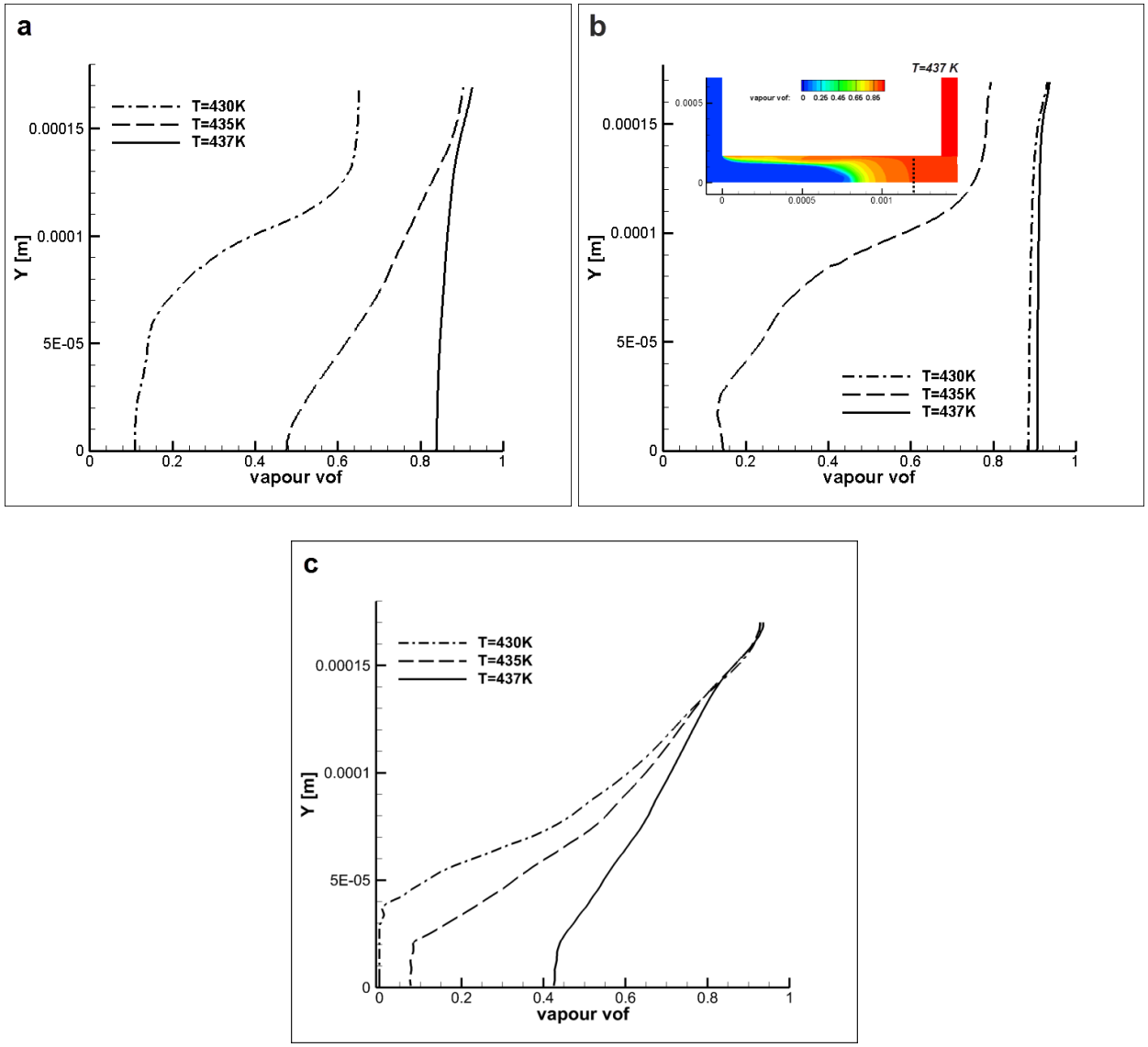

Fig. 11 Radial profile of the vapour volume fraction at X=0.0012m (87.5% of the nozzle length): (a) Model I, (b) Model II, (c) Model III.

Fig. 12 depicts the velocity fields, as predicted by the formulated hybrid models. The distinctive feature detected in the velocity fields corresponding to the high-temperature cases

(T=435K) is the flow transition to sonic velocity within the injector nozzle. In reference to the cases where the thermal term is neglected and thus flashing occurs outside the injector, it can be seen that the flow reaches sonic velocity at the outlet of the nozzle and accelerates immediately downstream. On the contrary, in the cases where significant flashing occurs within the nozzle, as the ones shown in Fig. 12, the flow velocity is sonic in a significant part of the nozzle, as indicated by the contours of the local speed of sound depicted as black lines on the figure, as well. Consequently, the fluid expansion downstream of the outlet is more intense, leading to more significant fluid acceleration. As also depicted on the contour plots of the velocity field (Fig. 9), the jet cone angle of the jet for the cases where flashing occurs is increased in comparison to the purely cavitating flows. These findings agree with the observations of Oza (1984), and Serras-Pereira et al. (2010) and Lamanna et al. (2014) referring to superheated jets entering a low-pressure chamber. The contour plots referring to Models I, II that predict a larger extent of the phase-change region in the channel core, depicted in Figs. 12a-b, indicate a higher fluid acceleration compared to Model III (Fig. 12c), an additional indication of the close connection between the phase and velocity fields. In all cases, it can be discerned that the jet, downstream of the outlet, expands in the radial direction, instead of having a pencil-shaped plume typical of flows with moderate in-nozzle nucleation. The most significant flow acceleration is predicted by Model I (Fig. 12a), which, if Fig. 11a is also taken into account, can be attributed to a significant part of the channel core ($Y<5\cdot10^{-5}$ m) being occupied by vapour with volume fraction values in the order of 0.5-0.6. This leads to adjustment of the speed of sound within the nozzle to values close to the minimum obtainable (see also Eq. 2) and thus to more significant flow acceleration downstream of it.

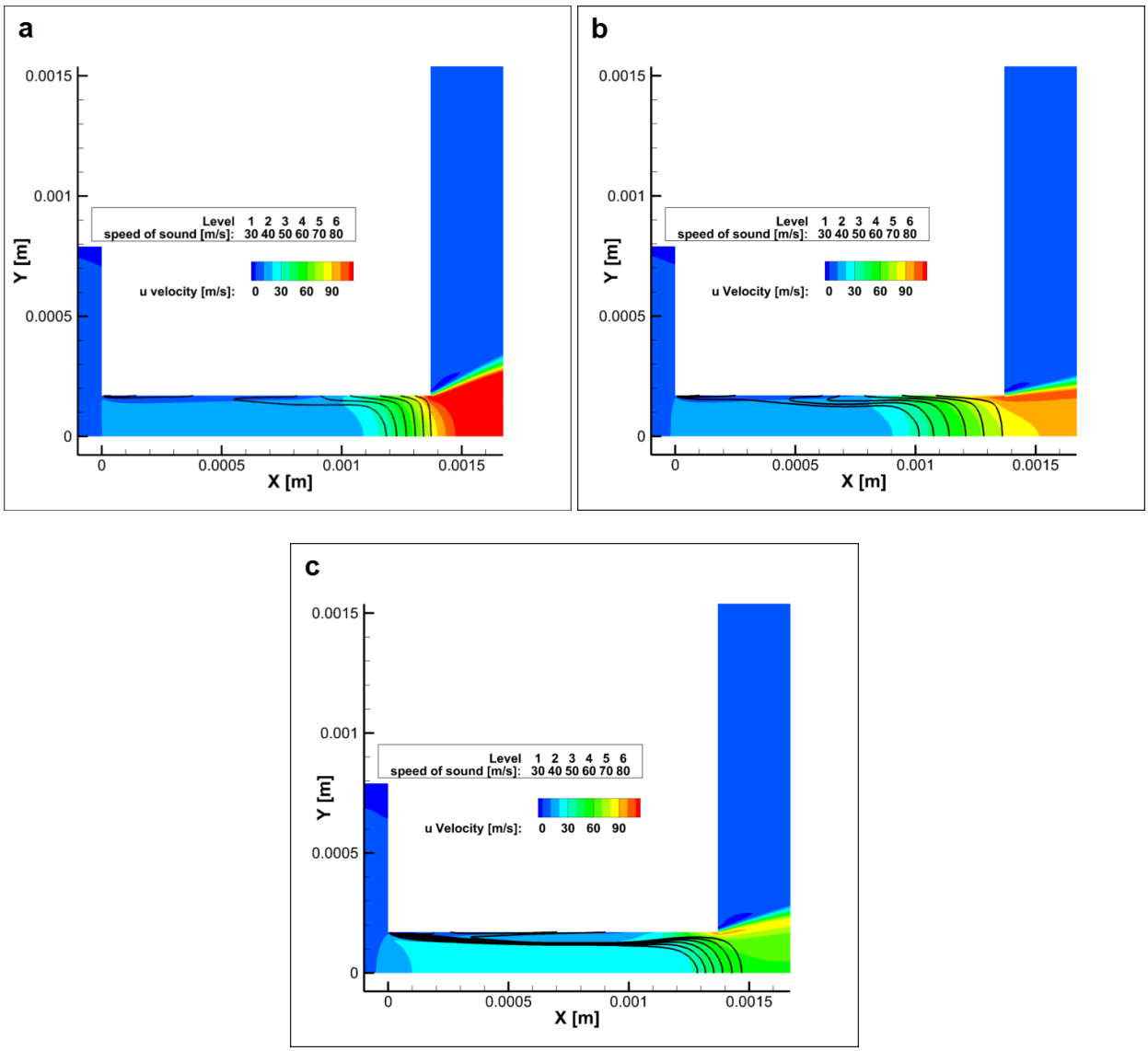

Fig. 12 Contours plots of the velocity field in the nozzle region (T=435K): (a) Model I, (b) Model II, (c) Model III.

In reference to the high temperature case for T=435K, Fig. 13a depicts the Mach number distribution along the throttle axis in regions downstream of the nozzle outlet. Since the velocity field depicted on Fig. 12 has been produced considering an increased mass-transfer rate in comparison to the flow conditions for which the Mach number distribution is presented in Fig. 8, it is therefore expected the flow expansion downstream of the nozzle outlet to be more severe than

the case of Fig. 8 and, therefore, the Mach number to reach higher values constituting the flow supersonic. The peak values for the Mach number are encountered shortly downstream of the nozzle outlet and are equal to 1.65, 1.49 and 1.37, as predicted by Models I, II and III, respectively.

The pressure distribution along the throttle axis, as predicted by the three hybrid models is presented in Fig. 13b. First of all, as can be seen Models I and II predict a higher fluid pressure within the nozzle ($0 \leq X \leq 0.00137$ m) than model III. A more gradual depressurization can be detected for Model II, while according to the predictions of Model I, pressure reduces rapidly in the vicinity of the outlet and furthermore the pressure minimum associated with the formation of the shockwave is more pronounced compared to the other two models. Hence, the flow expansion is more severe, according to the results produced by model II and, thus, the most significant flow acceleration shown in Fig. 12a is justified.

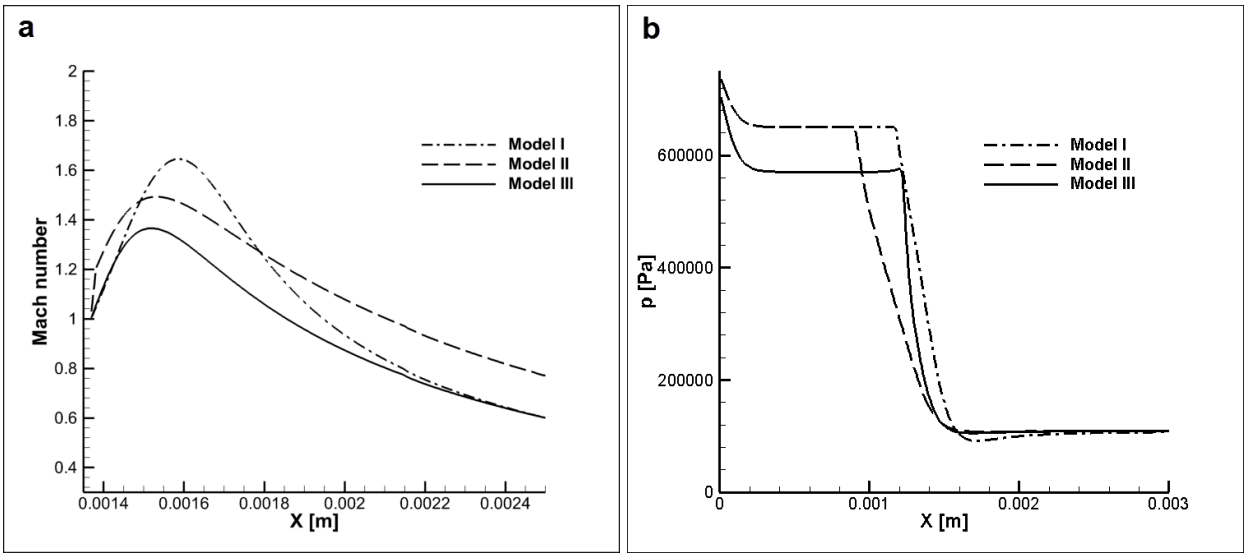

Fig. 13 (a) Mach number and (b) pressure distributions along the throttle axis (Y=0.0).

Finally, contour plots of the Jakob number, as predicted by Model III are presented in Fig. 14, in order to illustrate the relative magnitude of the weighting factor, Eq. (13), employed in the

formulation of the specific model. As can be seen, the Jakob number, obtains values in the order of 1.0 in the largest part of the throttle for T=430K (Fig. 14a), while higher values in the order of 3.0 can be detected for the higher temperature cases (Figs. 14b-c). Hence, the mass-transfer rate is primarily designated by the thermal effects in the specific temperature range (430-437K). Moderately higher Jakob-number values compared to the fluid bulk are evident slightly downstream of the throttle vertex in all figures, implying a more considerable influence of inertial forces in that region. As elucidated by Fig. 6, the cavitation models predict that the cavity pocket sets in at that specific area, as well. However, even at the throttle outer-wall region, the Jakob-number values are lower than 12, indicating a deviation from thermodynamic equilibrium and hence the phase-change rate is mainly designated by the second (thermal) term on the right hand side of Eq. (12). Besides, the Jakob number obtains high values, in the order of 12, at the throttle-exit region due to the rapid liquid depressurization, which obviously leads to the reduction of the corresponding saturation temperature. Mass transfer is then limited to the maximum (inertial) rate.

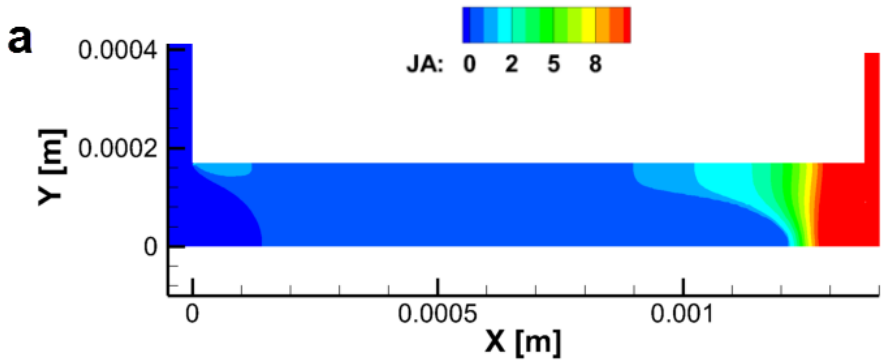

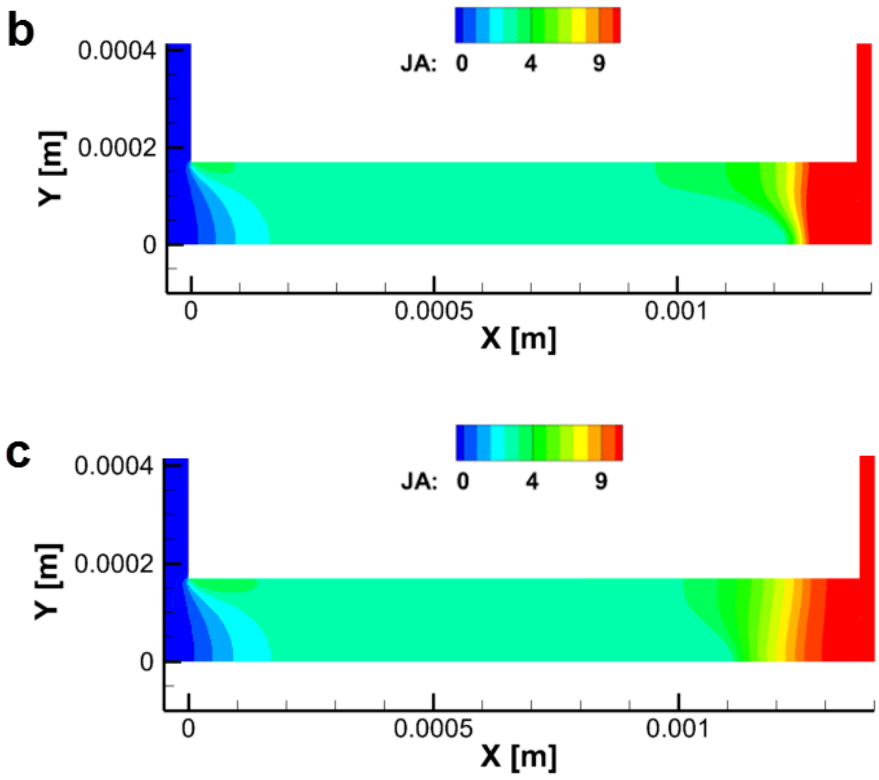

Fig. 14 Contour plots of the Jakob-number distribution in the throttle region (Model III): (a) T=430K, (b) T=435K and (c) T=437K.

3.3 Temperature field

In the case of a flashing jet, it is expected that the jet core will be subjected to cooling due to the subtraction of latent heat. In fact, the temperature drop will be more significant in the liquid regions where the mass transfer rate is higher. In other words, the superheated liquid transits to its saturation temperature, a condition of thermodynamic equilibrium, as the vapor bubbles grow, i.e. as the vapour volume fraction increases. The experimental work of Miyatake et al. (Miyatake et al. 1981) has showed that the rate of cooling increases for higher degrees of superheat.

As illustrated by the contour plots of the temperature field at T=430K (Fig. 15a), the jet cooling actually commences close to the injector outlet, while there is a localized strike of cold fluid with a temperature approximately equal to 415K in the area of increased mass-transfer rate. However, the cooling at the jet liquid core within the nozzle is in the order of 4K, which is deemed as negligible, since the jet discharges into a chamber with a set temperature of 373K. The plot corresponding to a higher degree of superheat (T=435K) depicted in Fig. 15b, illustrates a temperature field similar to that shown in Fig. 15a with the liquid-core cooling within the nozzle being in the order of 6K. It is therefore valid to deduce, that the effect of cooling does not have a considering impact on the emerging flow field and thus the solution of the energy equation could be avoided, thus reducing the computational cost.

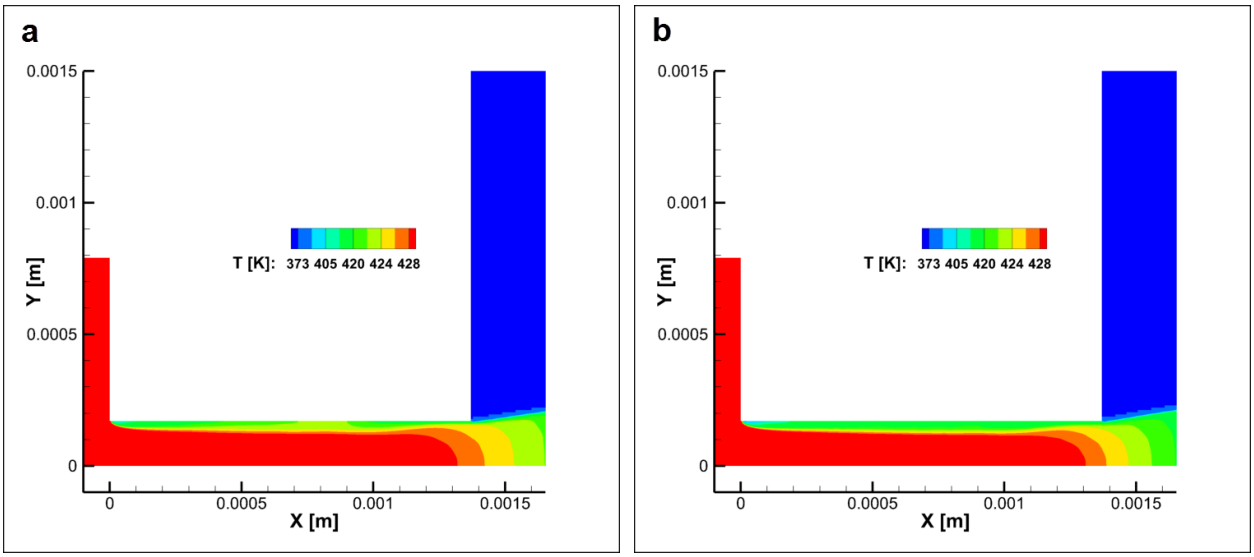

Fig. 15 Contour plots of the temperature field in the nozzle region (Model III): (a) T=430K, (b) T=435K.

4. Conclusions

The distinct flow features associated with the occurrence of flash boiling in an injector device have been elucidated in the present numerical investigation. A number of pure-cavitation and "hybrid" models, which also take into account the additional effect of thermal non-equilibrium conditions on the mass-transfer rate, were evaluated using a benchmark nozzle configuration for which experimental data have been reported. For the conditions reported by Reitz [15], the comparison of the predictions produced by the cavitation models with the experimental data revealed that the mass transfer is moderate within the nozzle owing to the relatively small number of nucleation sites estimated to be equal to 10^9 nucleation sites pre liquid volume unity.

The predictions of the formulated "hybrid" models, revealed a more extensive mass-transfer region within the injector in comparison to pure cavitation, as vapour-fraction values in the order of 0.20-0.40 were detected in the nozzle core as well, away from the region where the attached cavity sets in. It can be deduced that intense in-nozzle phase-change is possible to commence regarding the nozzle geometry investigated even for relatively low degrees of superheat in the range of 1.5-3.0K, considering the examined flow conditions. As, expected the phase change rate is proportional to the degree of superheat, i.e. the liquid temperature. The numerical results have clearly demonstrated that the occurrence of flash boiling within the injector is associated with chocked flow conditions (Mach number equal to unity) at the injector outlet and flow acceleration downstream of it, with flow velocities reaching values up to 120 m/s compared to a velocity of 40 m/s detected for purely cavitating flow. The acceleration of the jet exiting the nozzle, along with the fact that the fluid retains high pressure values in the order of 600-650 kPa within the nozzle, for the high temperature cases considered (T>435K), constitute clear proof that the flashing flow

is under-expanded within the nozzle, an observation in agreement with the findings of Oza (1984), and its expansion is associated with the formation of a shockwave downstream the injector outlet and high jet cone angle.

Acknowledgments

The research leading to these results has received funding from the People Programme (IAPP Marie Curie Actions) of the European Union's Seventh Framework Programme FP7/2007-2013/ under REA grant agreement n. 324313.

References

Aleiferis, P.G., Serras-Pereira, J., Augoye, A., Davies, T.J., R. F. Cracknell, and D. Richardson, Effect of Fuel Temperature on In-nozzle Cavitation and Spray Formation of Liquid Hydrocarbons and Alcohols from a Real-size Optical Injector for Direct-Injection Spark-Ignition Engines, *Int. J. Heat Mass Transf.*, vol. 53, no. 21–22, pp. 4588–4606, 2010.

Andriotis, A., Gavaises, M. and Arcoumanis, C., Vortex flow and cavitation in diesel injector nozzles *J. Fluid Mech.*, vol. 610**,** pp. 195–215, 2008.

ANSYS FLUENT, *Theory Guide V14.5*, pp. 724–746, 2012.

Battistoni, M., Duke, D.J., Swantek, A.B., Tilocco, F.Z., Powell, C.F., Som, S., Effects of noncondensable gas on cavitating nozzles, *Atomiz. Sprays*, vol. 25, no. 6, pp. 453–483, 2015.

Battistoni M., Som, S., Longman, D.E., Comparison of mixture and multifiuid models for in-nozzle cavitation prediction, *J. Eng. Gas Turb. Power*, vol. 136, 061506-1, 2014.

Brennen, C.E., *Cavitation and Bubble Dynamics*, Oxford University Press, Available at http://authors.library.caltech.edu/25017/1/cavbubdynam.pdf, 1995.

Brennen, C.E., *Fundamentals of Multiphase Flows*, Cambridge University Press, p. 100-108, 2005.

Chan, Q. N., Bao, Y., and Kook, S. "Effects of Injection Pressure on the Structural Transformation of Flash-Boiling Sprays of Gasoline and Ethanol in a Spark-Ignition Direct-Injection (SIDI) engine, *Fuel*, vol. 130, pp. 228–240, 2014.

Chang, D.L., and Lee, C.F., Preliminary Computational Studies of Flash Boiling for Fuel Injectors in Gasoline Direct Injection Automotive Engines, *Proc. of 37th lnter. Energy Conv. Eng. Conf.*, 2002.

Coutier-Delgosha, O., Reboud, J. L. and Delannoy, Y., Numerical simulation of the unsteady behaviour of cavitating flows, *Int. J. Num. Methods Fluids*, vol. 42, no. 5, pp. 527-548, 2003.

Forster, H. K., and Zuber, N., Dynamics of Vapor Bubbles and Boiling Heat Transfer, *AIChE Annu. Meet.*, vol. 1, no. 4, pp. 531–535, 1955.

Edelbauer, W., Strucl, J. and Morozov, A. Large Eddy Simulation of cavitating throttle flow, *Proc. SimHydro 2014:Modelling of rapid transitory flows*, Sophia Antipolis, 2014.

Franc, J.P. and Michel, J.M., Eds., *Fundamentals of Cavitation*, New York: Kluwer Academic Publishers, pp.165-168, 2005.

Gopalakrishnan, S. and Schmidt, D.P., Multidimensional Simulation of Flash-Boiling Fuels in Injector Nozzles, *Proc. ILASS Americas*, 2008.

Habchi C., A Gibbs Energy Relaxation Model for Cavitation Simulation, *Atomiz. Sprays*, vol. 25, no. 4, pp. 317–334, 2015.

Jones, O.C. and Zuber, N., Bubble Growth in Variable Pressure Fields, *J. of Heat Transfer*, vol. 100, no. 3, p.453-459, 1978.

Koukouvinis P., Gavaises M., Li, J. and Wang L., Large Eddy Simulation of Diesel injector including cavitation effects and correlation to erosion damage, *Fuel*, vol. 175, pp. 26-39, 2016

Lamanna, G., Kamoun, H., Weigand, B., and Steelant, J., Towards a Unified Treatment of Fully Flashing Sprays, *Int. J. Multiph. Flow*, vol. 58, pp. 168–184, 2014.

Lee, J., Madabhushi, R., Fotache, C., Gopalakrishnan, S., and Schmidt, D., Flashing Flow of Superheated Jet Fuel, *Proc. Combust. Inst.*, vol. 32, no. 2, pp. 3215–3222, 2009.

Miyatake, O., Tomimura, T., Ide, Y., Yuda, M., & Fujii, T. "Effect of Liquid Temperature on Spray Flash Evaporation," *Desalination*, vol. 37, no. 8, pp. 351–366, 1981.

Naseri H., Koukouvinis P. and M Gavaises M., Evaluation of Turbulence Models Performance in Predicting Incipient Cavitation in an Enlarged Step-Nozzle, *J. Phys. Conf. Ser.*, 012095, 2015.

Negro, S., and Bianchi, G. M., Superheated Fuel Injection Modeling: An Engineering Approach, *Int. J. Therm. Sci.*, vol. 50, no. 8, pp. 1460–1471, 2011.

Oza, R. D., On the Mechanism of Flashing Injection of Initially Subcooled Fuels, *J. Fluids Eng.*, vol. 106, no.1, pp. 105-109, 1984.

Papadopoulos, N. and Aleiferis, P., Numerical modelling of the in-nozzle flow of a diesel Injector with moving needle during and after the end of a full injection event, *SAE Int. J. Engines*, vol. 8, no. 5, 2015.

Price, C., Hamzehloo, A., Aleiferis, P. and Richardson, D., Aspects of Numerical Modelling of Flash-Boiling Fuel Sprays Flash-Boiling Atomization, *SAE Tech. Pap.*, 2015-24-2463, 2015.

Prosperetti, A., and Plesset, M. S., Vapour-bubble growth in a superheated liquid, *J. Fluid Mech.*, vol. 85, no. 02, p. 349-368, 1978.

Prudhomme, S.M. and Haj-Hariri, H., Investigation of supersonic underexpanded jets using adaptive unstructured finite elements, Fin. Elem. Anal. Design, vol. 17, pp. 21-40, 1994.

Reitz, R. D., A Photographic Study of Flash-Boiling Atomization, *Aerosol Sci. Technol.*, vol. 12, no. 3, pp. 561–569, 1990.

Robinson A.J., *Bubble Growth Dynamics In Boiling*, PhD Thesis, McMaster University, 2002.

Saha, K., Som, S., Battistoni, M., Li, Y., Quan, S. and Senecal, P. K., Numerical Simulation of Internal and Near-Nozzle Flow of a Gasoline Direct Injection Fuel Injector, *J. Phys. Conf. Ser.*, vol. 656, p. 012100, 2015.

Schmidt D.P., Gopalakrishnan. H. and Jasak, H., Multi-dimensional simulation of thermal non-equilibrium channel flow, *Int. J. Multiph. Flows*, vol. 36, pp. 284-292, 2010.

Scriven, I. E., On the Dynamics of Phase Growth, Chem. Eng. Sci., vol. 10, no. 1-2, pp. 1-13, 1959.

Senda, J. and Hojyo, Y., Modeling on Atomization and Vaporization Process in Flash Boiling Spray," *JSAE Review*, vol. 15, pp. 291–296, 1994

Serras-Pereira, J., Van Romunde, Z., Aleiferis, P.G., Richardson, D., Wallace, S. and Cracknell, R.F., Cavitation, Primary Break-up and Flash Boiling of Gasoline, iso-Octane and n-Pentane with a Real-size Optical Direct-Injection Nozzle, Fuel, vol. 89, pp. 2592–2607, 2010.

Sher, E., Bar-Kohany, T., and Rashkovan, A., Flash-Boiling Atomization, *Prog. Energy Combust. Sci.*, vol. 34, no. 4, pp. 417–439, 2008.

Singhal, A.K., Athavale, M.M., Li, H., and Jiang, Y., Mathematical Basis and Validation of the Full Cavitation Model, *J. Fluids Eng.*, vol. 124, no. 3, p. 617-624, 2002.

Sou, A., Hosokawa, S., Tomiyama A., Effects of cavitation in a nozzle on liquid jet atomization, Int. J. Heat Mass Transf., vol. 50, pp. 3575–3582, 2007.

Theofanous, T., Biasi, L., Isbin, H. S. and Fauske, H., A Theoretical Study on Bubble Growth in Constant and Time-Dependent Pressure Fields, *Chem. Eng. Sci.*, vol. 24, no. 5, pp. 885–897, 1969.

Yuan, W., Sauer, J., and Schnerr, G.H., Modeling and Computation of Unsteady Cavitation Flows in Injection Nozzles," *Mec. Ind.*, vol. 2, pp. 383–394, 2001.

Vieira, M.M. and Simões-Moreira, J.R. Low-Pressure Flashing Mechanisms in iso-Octane Liquid Jets, *J. Fluid Mech.*, vol. 572, p. 121-144, 2007.

Wagner, W., and Pruss, A., The IAPWS Formulation 1995 for the Thermodynamic Properties of Ordinary Water Substance for General and Scientific Use, *J. Phys. Chem. Ref. Data*, vol. 31, no. 2, 2002.

Zhang, Y., Li, S., B. Zheng, J. Wu, and B. Xu, "Quantitative Observation on Breakup of Superheated Liquid Jet Using Transparent Slit Nozzle," *Exp. Therm. Fluid Sci.*, vol. 63, pp. 84–90, 2015.

Zwart, P.J., Gerber, A.G. and Belamri, T., A Two-Phase Flow Model for Predicting Cavitation Dynamics, *Proc. of 5th Int. Conf. on Multiph. Flow*, 2004.

Zwick, S.A. and Plesset, M.S., On the Dynamics of Small Vapor Bubbles in Liquids, *J. Math. Phys.*, vol. 33, no. 1, pp. 308-330, 1955.